TSUNAMIGENIC SOURCE MECHANISM AND EFFICIENCY OF THE MARCH 11, 2011 SANRIKU EARTHQUAKE IN JAPAN

George Pararas-Carayannis

Tsunami Society International, Honolulu, Hawaii, USA
drgeorgepc@yahoo.com

ABSTRACT

The great Tohoku earthquake of March 11, 2011 generated a very destructive and anomalously high tsunami. To understand its source mechanism, an examination was undertaken of the seismotectonics of the region and of the earthquake' focal mechanism, energy release, rupture patterns and spatial and temporal sequencing and clustering of major aftershocks. It was determined that the great tsunami resulted from a combination of crustal deformations of the ocean floor due to up-thrust tectonic motions, augmented by additional uplift due to the quake's slow and long rupturing process, as well as to large coseismic lateral movements which compressed and deformed the compacted sediments along the accretionary prism of the overriding plane. The deformation occurred randomly and non-uniformly along parallel normal faults and along oblique, en-echelon faults to the earthquake's overall rupture direction – the latter failing in a sequential bookshelf manner with variable slip angles. As the 1992 Nicaragua and the 2004 Sumatra earthquakes demonstrated, such bookshelf failures of sedimentary layers could contribute to anomalously high tsunamis. As with the 1896 tsunami, additional ocean floor deformation and uplift of the sediments was responsible for the higher waves generated by the 2011 earthquake. The efficiency of tsunami generation was greater along the shallow eastern segment of the fault off the Miyagi Prefecture where most of the energy release of the earthquake and the deformations occurred, while the segment off the Ibaraki Prefecture – where the rupture process was rapid – released less seismic energy, resulted in less compaction and deformation of sedimentary layers and thus to a tsunami of lesser offshore height. The greater tsunamigenic efficiency of the 2011 earthquake and high degree of the tsunami's destructiveness

along Honshu's coastlines resulted from vertical crustal displacements of more than 10 meters due to up-thrust faulting and from lateral compression and folding of sedimentary layers in an east-southeast direction which contributed additional uplift estimated about 7 meters - mainly along the leading segment of the accretionary prism of the overriding tectonic plate.

Keywords - *Japan; Honshu; Sanriku; earthquake; seismotectonics; tsunami; source-mechanism; tsunamigenic efficiency; Japan Trench.*

I.   INTRODUCTION

The most powerful earthquake in Japan in recent years occurred on March 11, 2011 off the coast of Sanriku (which includes the Aomori, Iwate, and Miyagi prefectures) (Fig. 1). It was one of five great earthquakes in the world since 1900. It generated a Pacific-wide, tsunami, which was particularly devastating and anomalously high along the northeast coast of Honshu. Warnings were issued for more than 20 countries and Pacific islands.
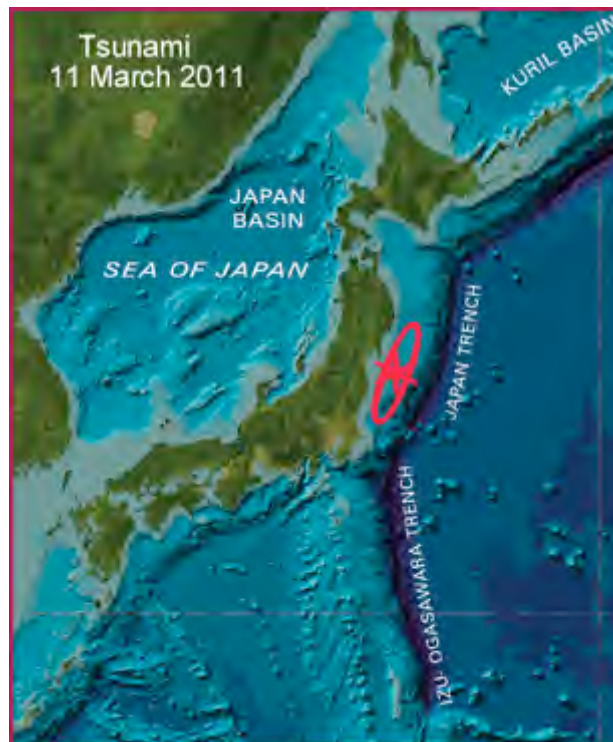
Fig. 1. Epicenter of the March 11, 2011 Earthquake; Tsunami Generating Area; Major Basins and Trenches

In Japan, both the earthquake and the tsunami caused extensive and severe damage to roads and railways, ignited fires and triggered a dam collapse. Many electrical generators were taken down. Most of the destruction and deaths in Japan were caused by the tsunami. As of April 18, 2011 the

death toll in Japan had risen to 13,843, another 14,030 people remained missing and another 136,481 were displaced (Japan's National Police Agency). The disaster left about 4.4 million homes in northeastern Japan without electricity and 1.4 million without water. There were power outages for about 4 million homes in Tokyo and the surrounding areas. Early estimates indicated that the monetary losses would exceed $100 billion.

To understand the tsunami's generation mechanism and the cause of the extreme wave heights along northeast Honshu, an investigation was undertaken of the seismotectonics of the region and of the earthquake's focal mechanism, rupture patterns and spatial and temporal sequencing and clustering of major aftershocks – the latter defining the limits of crustal displacements and the amount of energy release. Evaluation of the tsunamigenic efficiency includes a review of the combined earthquake rupturing impact on both the subducting oceanic lithosphere and on the overriding plate, as well as examination of other large vertical and lateral displacements that contributed to the tsunami's anomalous height. Additionally evaluated are the temporal elastic deformations caused by faulting and the collateral impact of lateral compression on the sediments on the accretionary wedge near the trench axis. Finally, the 2011 tsunami source mechanism is compared with those of previous destructive events in 1896 and 1933 for the purpose of evaluating similarities of factors that contributed to the enhancement of the tsunami's height and destructiveness.

2. THE EARTHQUAKE AND THE TSUNAMI

2.1 The Earthquake

The March 11, 2011 earthquake occurred at 05:46 UTC, 14:46 JST (local time). The quake epicenter was at 37.68N; 143.03E (USGS) was about 373 kilometers (231 miles) away from Tokyo, about 130 kms (81 mi) off the east coast of Oshika Peninsula and about 150 km west of the tectonic boundary of the Eurasian and Pacific plates, characterized by the Japan Trench (Fig. 1). Strong ground motions were felt as far away as Tokyo. The Moment Magnitude was initially estimated at Mw=8.9 (USGS) but later revised upward to Mw=9.0. However, based on long period surface waves (ranging from 166 to 333 seconds), the total seismic moment was recalculated to be about 5.6x10^22 Nm, corresponding to a moment magnitude of 9.1 - almost as much as that of the 2004 Sumatra earthquake (Mw 9.15). The focal depth was 15.2 miles (24.4 kms) (USGS). Focal mechanism analysis indicated a low angle nodal plane with a strike of 199^0, a dip angle of 10^0 and a slip angle of 92^0 (Shao et al., 2011).

2.2 The Tsunami

2.2.1 Near and Far Field Tsunami Impact

The near and far field effects of the tsunami and the quantitative runup heights have been reported in the literature and in preliminary Internet summaries (Pararas-Carayannis, 2011).

Near-Field Effects - Waves began striking the shores of Sanriku a few minutes after the quake. The impact was particularly devastating along coastal areas of northeastern coastal areas of Honshu, where the irregular coastline and numerous bays amplified the tsunami height and its destructiveness.

Tsunami Wave Heights (m)

Aomori 12.0
16.0
18.3
18.1
29.0
20.2
Iwate Taro 14.6
18.9
15.0
10.7
16.7
Ryori 38.2
18.0
26.7
Miyagi

Hardest hit was the Miyagi Prefecture (Fig. 2). In some areas the waves inundated as far as 10 kms (6 miles) inland. Further south, at the Fukushima Daiichi Nuclear Power Plant, a 19-foot high protective levee was overtopped by the tsunami, which submerged the lower height structures including the diesel generators and knocked out regular and backup cooling systems. The maximum tsunami wave height was ~46 feet. A 150-foot high splash was photographed as the tsunami impacted the turbine building of the plant, passing over its roof and striking the adjacent reactor building. Four of the plant's six reactors suffered damage to their radioactive cores. A state of emergency was declared which required massive evacuation of more than 200,000 residents living within a 20 km (12 mi) radius.

Fig. 2 Reported Maximum Tsunami Heights in meters along the Sanriku coast.

Reported run-up heights ranged up to 25.5m, but at Koborinai the maximum runup reached 37.9 meters (124 feet). A fire was ignited at an oil refinery in Chiba Prefecture near Tokyo. At Rikuzentakata the maximum tsunami wave was 13 meters high and overtopped the existing protective tsunami seawall, which was 6.5 meters high. The tsunami reshaped the entire coastline and flooded the agricultural fields further north. Along the Taru District the tsunami overtopped the protective seawall and caused extreme destruction. Reported run-up heights ranged form 19.5m to 25.5m. At Ryori Bay-Shirahama, the tsunami run-up height reached 23.60 meters. At the fishing village of Ryoishi the waves destroyed part of the 9-meter (30-foot) protective tsunami wall or simply overtopped it completely destroying everything in the way. At Iwate, the GPS ocean gauge located in 204 meters depth in the offshore area measured a 6.7 meters (22 ft) tsunami height. At Miyako, waves of 11.5 meter overtopped the existing tsunami barrier and seawall, which was 7.6 meters high. The tide gauge recorded a tsunami height of 8.5 meters. However, run-up heights of as much as 19.5 and 25.5 meters were reported from this area.

At Natori, the tsunami height was 12 meter near Sendai airport and 9 meters high near the fishing port. At Kesennuma, the wave heights ranged from 9.10 to 14.7 meters. At Kamaishi, the waves ranged from 7-9 meters in height. The maximum tsunami height at Ofunato was 8.0 meters and at Arahama 9.3 meters. At Ishinomaki, the tsunami was 5 meter high in the harbor but runup reached 16

meters at Ogachi-machi.   At Kashima Port, 4.22 meter and 5.2 meter tsunami heights were observed. At Fudai, 3,000 residents survived because of a 51-foot (15.5 meter) floodgate. However, the tsunami run-up at the towers of the floodgate reached 66 feet (20 meters). At Ishinomaki City the tsunami was over 10 feet high and washed homes away.

   Far-Field Effects – The tsunami's energy flux radiated across the Pacific and caused extensive destruction at distant shores in the Hawaiian Islands, California, Oregon, Chile and elsewhere (Fig. 3). Figure 2 provides the tsunami travel times and the location of DART and of coastal tide stations.

   Vanuatu - The tide gauge measured 1.88 meters (6.2 feet).

   Hawaiian Islands – Maximum runup heights ranged from 2 to 3 meters (7 to 11 feet) on the islands of Maui and Hawaii (the Big Island). Four waves struck Midway Atoll at the Northwest end of the Hawaiian Islands. The highest wave reached a height of nearly 5 feet and completely washed out the reef and Spit Island, the smallest in the atoll. The tide gauge measured 1.27 meters (4.2 feet). According to reports the tsunami killed hundreds of birds and swept away nests protecting seabird chicks, which were unable to fly. Reportedly, 110,000 Layson and black-footed albatross chicks were killed, along with 2,000 adult birds.
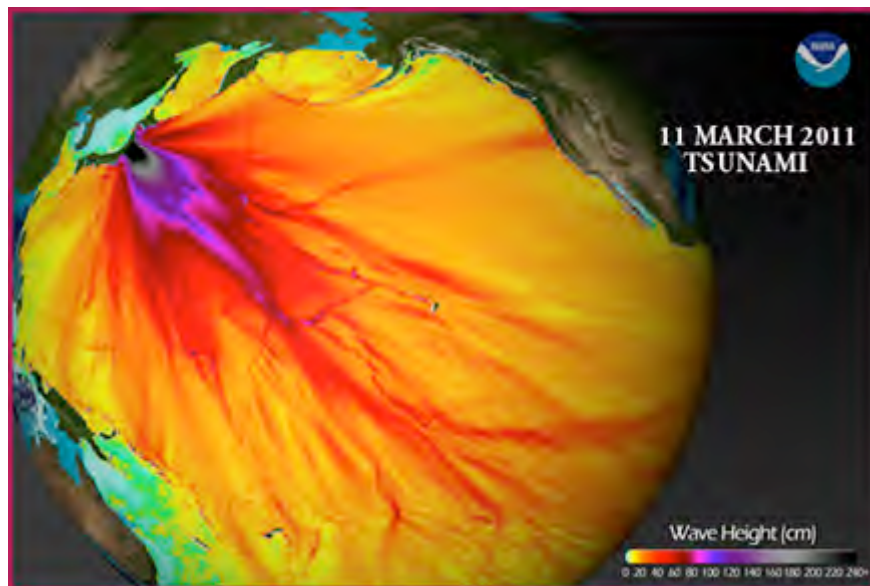

Fig.3. *Tsunami Energy Propagation Across the Pacific (NOAA graphic)*.

Damage to boats on the island of Oahu was extensive. Kahului on the Island of Maui suffered the worst damage. The tide gauge there measured 1.74 meters (5.7 feet). On the Island of Hawaii, there was flooding and minimal damage of a hotel lobby near Kealakekua Bay. The Hilo tide gauge measured a 0.69 meters (2.3 feet) high wave.

California - There was damage to docks and boats. At Crescent City, tsunami waves did extensive damage to port docks and severely damaged 35 boats. The reported maximum wave height was estimated at 2.5 meters. The tide gauge measured a wave of 2.02 meters (6.6 feet) high. The tsunami caused also extensive damage at Santa Cruz Harbor, estimated at more than 2 million dollars.

Oregon - Wave heights were relatively small, ranging from .90 and 1.20 (3 to 4 feet). Wave periods ranged from 10-15 minutes.

Chile – There were reports of major damage. Maximum-recorded tsunami runup at Coquimbo was 2.55 meters, at Caldera 2.43 meters and at Talcahuano 2.15 meters.

3. SEISMOTECTONICS OF THE REGION

Active tectonic convergence of the Pacific plate with the Eurasian and North American plates has created an extensive and complex tectonic plate margin along the Japanese island group. The following is a brief overview of the seismotectonics of the region.

3.1 Tectonic Evolution

Japan was originally the coastal part of Eastern Eurasia. However, many hundreds of millions of years ago (from mid-Silurian to the Pleistocene) oceanic crust movements caused by subduction processes began pulling Japan away from the continental block. About 15 million years ago these processes begun to open the Sea of Japan - a complex basin between Japan and the Korea/Okhotsk Sea Basin - which represents another sub plate with apparent counter clock rotational movement as it interacts against the Okhotsk plate along the inland sea boundary of the Hidaka Collision Zone (HCZ) (Fig. 4).

Fig. 4. The postulated Amurian Microplate (Modified after Wei and Seno, 1998)

Thus, a separate Amurian microplate has been postulated (Wei and Seno, 1998). Two earthquakes in 1983 and 1993 in the eastern boundary of this microplate generated destructive tsunamis in the Sea of Japan basin. Furthermore, Sakhalin Island, north of Hokkaido, which separates the Sea of Japan from the Sea of Okhotsk, is probably the result of transpressional tectonics along the North America-Eurasia boundary (Pararas-Carayannis, 1983,1994). However, whether the Okhotsk plate and Northern Honshu is part of the North American plate or not, has not been ascertained (Seno et al., 1981). Similarly, whether Honshu is part of the North America plate, of the Eurasian plate or an independent microplate has not been determined.

In brief, Japan is a mature island arc. Subduction of the Philippine Sea Plate beneath the continental Amurian Plate, the Okinawa Plate to the south and of the Pacific Plate under the Okhotsk Plate to the north, continues to the present day and is the cause of frequent earthquakes, tsunamis and of occasional volcanic eruptions. The convergence rate across the boundary between the Pacific and Eurasian tectonic plates along the east side of Honshu Island varies from about 8 to 9 cm/year (3.1 to 3.5 in). As the Pacific plate subducts under Honshu, the high convergence results in the build-up of stresses. Arc stresses contribute to back-arc spreading (Seno & Yamanaka, 1998). After reaching aseismically a threshold of elastic deformation, the stresses are suddenly released by earthquakes. Large tsunamigenic earthquakes occur periodically near the eastern tectonic boundary characterized by the Japan Trench as the western edge of the Pacific Plate subducts under Honshu. Destructive tsunamis are generated from large earthquakes either on the outer ridge of the subducting plate or on the overriding plate, west of the Japan Trench – where the extensive forearc and accretionary sedimentary wedge seem to have significant effects on the type of boundary slips that can be expected and on the frequency and intensity of tsunami-earthquakes.

3.2 Seismicity of Japan

Japan accounts for about 20 per cent of the world's earthquakes. Its high seismicity (Fig. 5) results from compression along the Pacific-North America subduction zone, from outer rise and intra-plate events and from magmatic effects of plumes or super plumes which may have hydrated the subducting oceanic lithosphere (Pararas-Carayannis, 1994; Seno & Yamanaka, 1996). Usually, shallow normal faulting occurs in the trench-outer rise region, as well as on the overriding Eurasian plate and the outer slope of the Japan Trench (Seno & Gonzalez, 1987).

Seismicity of Honshu - Along the northern segment of the Honshu arc, there is a triple seismic zone with variable degrees of seismicity due to regional stress fields (Kewakatsu & Seno, 1983; Seno & Takano, 1996; Seno, 1999b) (Fig. 6). It has been proposed that northern Honshu may be a separate microplate (Seno, 1999a). It has also been postulated that the subduction zone off Miyage Prefecture – where the 2011 tsunami was anomalously high – has a double zone of seismicity (Seno & Pongsawat, 1981; Seno & Kroeger, 1983).

Small earthquakes occur frequently along the east side of Honshu. Stronger earthquakes of M6.0 and large earthquake M7.0 occur less frequently and intermittently. Such earthquakes usually result from normal-types of faulting in areas where the shear stress is predominant - thus less likely to
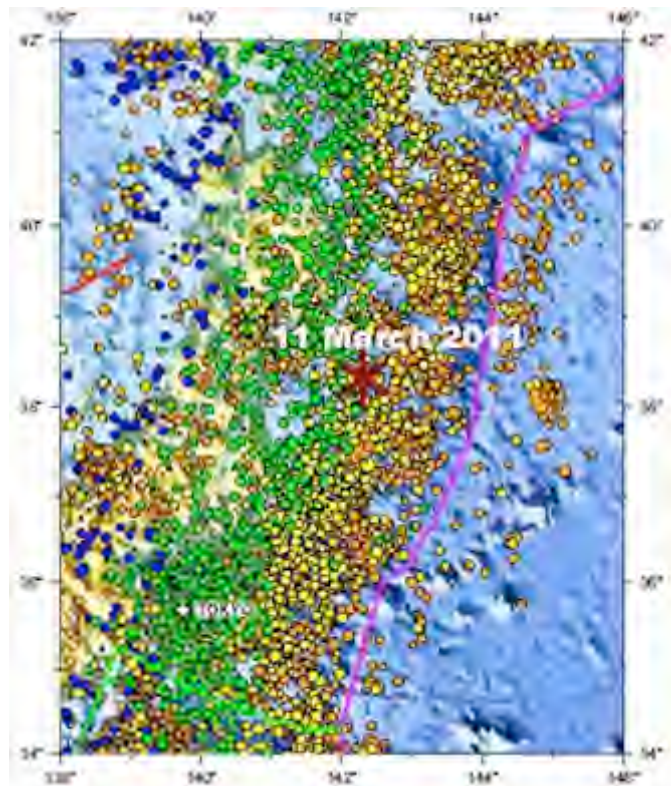
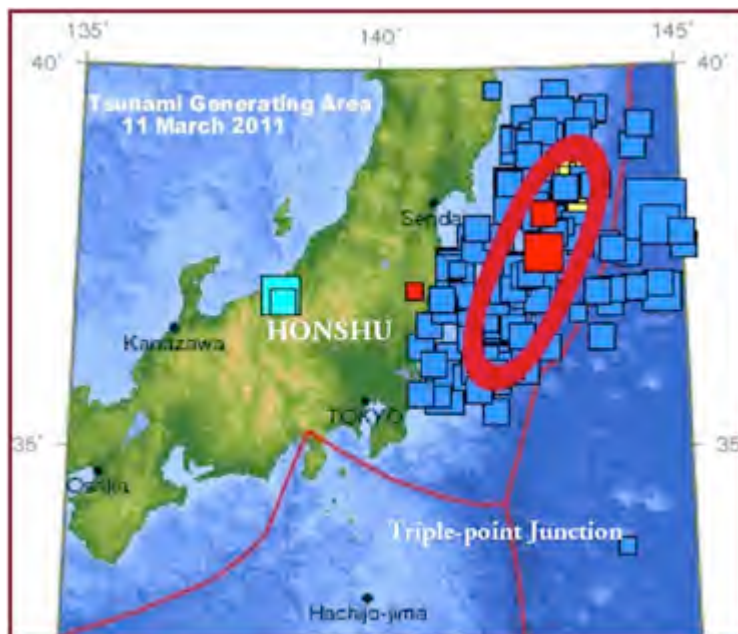*Fig. 5. Seismicity of Japan. Epicenter of the 11 March 2011 earthquake.*

Fig. 6. Aftershocks and Tsunami Generating Area (Modified USGS mapping of major aftershocks).

generate great tsunamis. Earthquakes of M8.0 or greater occur infrequently on the average every 50 to 100 years. Such mega-thrust earthquakes involve mainly a mechanism where the compressional stress is predominant and their large vertical displacements are the cause of destructive tsunamis. The great Meiji Sanriku earthquake of 1896 off the Tōhoku region was such an event. It generated a destructive tsunami with waves reaching as high as 38 meters along the Sanriku coast. Another earthquake known as the 1933 (Shōwa) Sanriku Earthquake, generated another destructive tsunami. The March 11, 2011 earthquake (Mw9.0) had many similarities with the 1896 event (Pararas-Carayannis, 2009; 2011). All such tsunamigenic events in the past were shallow (about 20 km focal depth) and involved a thrust mechanism of compressional stress, which resulted in the uplift of the overriding tectonic plate, as well as in great horizontal movements that disturbed the sedimentary layers on the accretionary prism.

4. PAST AND RECENT DESTRUCTIVE TSUNAMIS

The Sanriku coast in particular and other and areas in the Tōhoku region have been impacted by numerous large tsunamigenic earthquakes. The historic record shows that a total of 65 destructive tsunamis struck Japan between A.D. 684 and 1960 (Pararas-Carayannis, 1982; 2000). As early as 18 July 869 (also reported as July 13, 869), an earthquake with an estimated magnitude of 8.3 generated a tsunami along the Sanriku coast, which resulted in the loss of 1,000 lives and the destruction of hundreds of villages. On 3 August 1361, another tsunami destroyed 1,700 houses in this same area and killed a large number of people. On 20 September 1498, 1,000 houses were washed away and 500 deaths resulted from a tsunami, which struck the Kii peninsula. Kyushu was struck by a destructive tsunami in September 1596. Great loss of life occurred on 31 January 1596 from a tsunami on the island of Shikoku, affecting also a number of regions in Honshu.

On 2 December 1611 another destructive tsunami struck Keichō killing almost 3,000 people along the Sanriku coast. The same tsunami killed more than 3,000 people in the Nanbu-Tsugaru area. Another earthquake on 17 February 1793 generated a tsunami that struck the Sanriku coast killing a number of people. On August 23, 1856, a strong offshore earthquake off the Sanriku coast generated another destructive tsunami.

The great Meiji Sanriku earthquake of 15 June 1896 generated a tsunami, which resulted in 27,122 deaths, thousands of injuries and the loss of over 10,000 structures and of more than 7,000 boats and ships. On 3 March 1933 the Shōwa Sanriku Earthquake generated a tsunami that stuck the Sanriku area. The maximum wave height at Ryōri Bay was 28.7 meters. The waves killed more than 3,000 people, injured hundreds more and destroyed approximately 9,000 homes and 8,000 boats. In December 1944, another offshore earthquake near central Honshu generated a tsunami that caused almost 1,000 deaths and the destruction of over 3,000 houses. The Nankaido tsunami, on 21 December 1946, resulted in 1,500 deaths and the destruction of 1,151 houses (Pararas-Carayannis, 1982). The 11 March 2011 earthquake generated the most destructive tsunami in recent times in the same general area. Given the history of catastrophic tsunamis along the Sanriku region, this latest event was expected to occur – although its timing could not be forecasted.

5. TSUNAMI SOURCE MECHANISM

The March 11, 2011 quake had characteristics of severity of tsunami generation usually associated with slow rupture velocity within compacted, sedimentary layers. Because of their tsunamigenic efficiency, such events are known as tsunami earthquakes. The 2011 earthquake had a complex focal mechanism, which involved mainly reverse thrusting and compression, but also multiple parallel ruptures, as well as extensive lateral and vertical sediment displacements - which contributed to the tsunami's severity.

The present evaluation includes a review of the combined rupturing impact on both the subducting Pacific oceanic lithosphere and on the overriding Eurasian tectonic plate, as well as on the large vertical tectonic crustal displacements. Additionally examined are the spatial and time sequence of foreshock and aftershock distribution, the clustering of aftershocks, the three-dimensional dynamics of shallow and deeper subduction processes, the effects of temporal elastic deformation caused by faulting and the collateral impact on the sediments of the accretionary prism. Finally, a comparison is undertaken of source characteristics of the destructive tsunamis of 1896 and 1933 in the same general area off Sanriku's coastlines. Although the 2011 earthquake occurred slightly to the south of the 1896 event, it had many similar source characteristics. The similarities and differences are discussed in a subsequent section.

5.1 Examination of Foreshocks and Aftershocks

5.1.1 Foreshocks

The main earthquake was preceded on 9 March 2011 by a large Mw7.2, shallow (less than 30 km), foreshock, followed by three more with magnitude greater than 6. The large foreshock occurred at 38.42N, 42.83E a little north of the subsequent great earthquake of March 11. Subsequent aftershocks prior to the main earthquake, spread to the north, but several of the larger events appeared to have migrated towards the eventual nucleation region of the 11 March 2011 main earthquake, at 38.30N, 142.34E (USGS). None of the foreshocks generated a tsunami.

5.1.2 Aftershocks

Examination of aftershock distribution indicates that the seismic energy of the March 11, 2011 earthquake was mainly released about 100 km off the coast of Miyagi and Fukushima Prefectures. About fifty minutes following the main quake on March 11, there were a large number of aftershocks, the largest having a magnitude of 7.1 (Table 1). Shortly afterwards, 35 more aftershocks larger than magnitude 5.0 and 14 larger than magnitude 6 were recorded (UGSS). By mid-March 2011 more than 250 aftershocks with magnitudes of over 5.0 had occurred and 25 of these had magnitudes over 6.0. Strong, shallow aftershocks with magnitudes greater than 6 were recorded on March 27 and 28.

Table 1. Main Earthquake and Major Aftershocks in the First 71 minutes (Mw8.9 assigned to main earthquake – revised later to Mw9 and Mw9.1)

UTC DATE-TIME 2011/03/11	Mag	Lat deg	Long deg	Depth km
05:46:24	9	38.322	142.369	24.4
06:06:11	6.4	39.025	142.316	25.1
06:07:22	6.4	36.401	141.862	35.4
06:15:46	6.8	36.126	140.234	30.2
06:25:51	7.1	38.106	144.553	19.7
06:48:47	6.3	37.993	142.764	22.3
06:57:15	6.3	35.758	140.992	30.2

5.1.3 Clustering of Aftershocks

Cluster algorithm analysis of aftershocks in chronological sequence (Peter Zhol - personal communication), determined a big cluster of 260 events; a second cluster of 120 events and a third cluster of 60 events, as well as 20 very small clusters - typically one or two events each (Fig. 7).
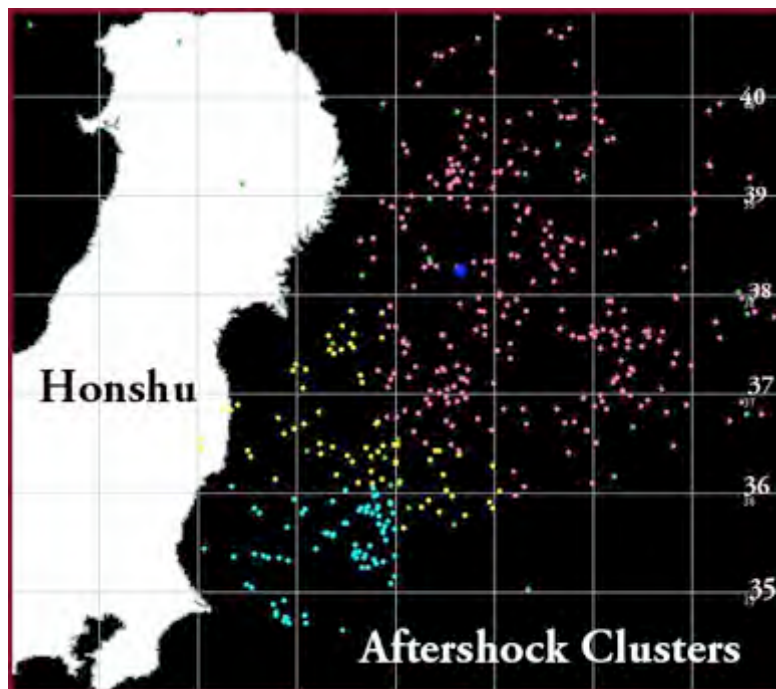

Fig. 7. Three Major Clusters of Aftershocks (*Depths (modified after Peter Zhol - personal communication*)

Many of the aftershocks may have occurred on unmapped, minor faults both in the intra-plate region as well as on the outer rise of the subducting plate. Plotting the aftershock focal depths along eastern Honshu indicated that there was a spectacular peak at a focal depth of about 24-25 km (Fig 8). The significance of this to tsunami generation was evaluated in terms of regional, spatial subduction geometry, slip, crustal movements and sediment displacements. Buckling of the crust due to subduction friction probably activated many minor, normal faults, which gave rise to subsequent aftershocks - even outside the tsunami generating region on the outer ridge of the subducting plate. Indeed the aftershock distribution was extensive, covering an area that was approximately 500 km long and 300 km wide.
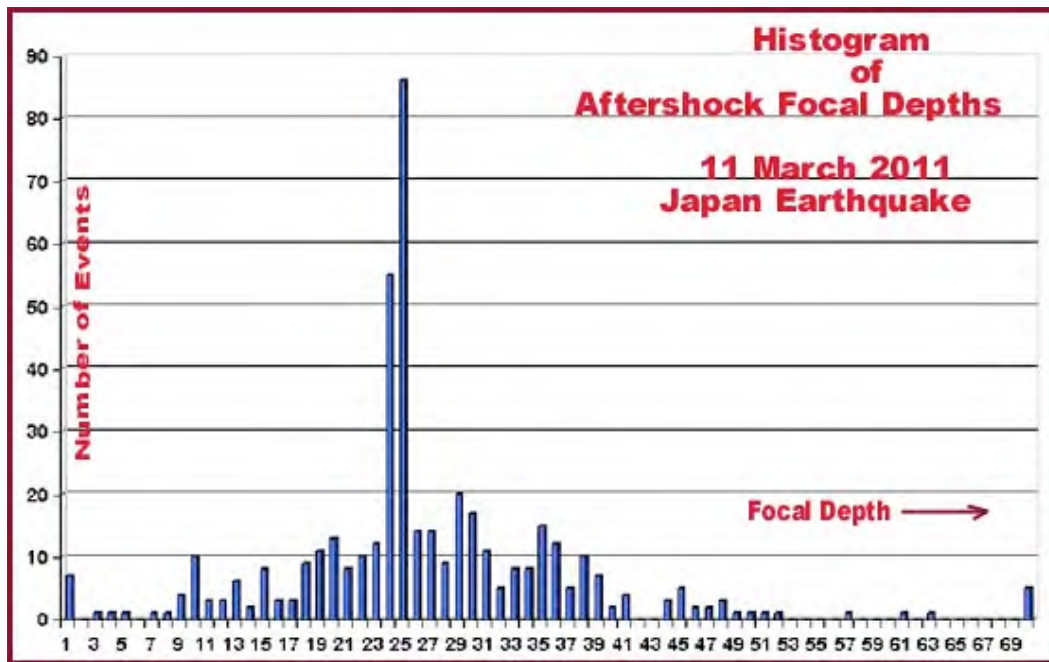

Fig. 8. Histogram of Aftershock Focal Depths (modified after Peter Zhol - personal communication)

5.1.4 Examination of Rupture Propagation and Duration

The effects of sediments on earthquake rupture velocity and tsunami generation for other subduction regions such as Makran in the North Arabian Sea, the Sunda Trench segment in the Andaman Sea and the Mid-America Trench have been examined (Pararas-Carayannis, 1992; 2005; 2006). In all these regions of subduction block motions of consolidated sediments were associated with bookshelf faulting, which contributed to slow-rupturing, silent and deadly tsunami-earthquakes. The block motions were extremely shallow and occurred within subducted sediments where there was a lot of shear - thus the rupture was slower in speed. In all of these cases, the degree of sediment consolidation along the plate boundary appeared to have been a key factor in locking slippage on the megathrust region of the tectonic boundary, then releasing greater energy when the stress thresholds were exceeded.

Apparently, the region where the 11 March 2011 Tohoku earthquake occurred had reached a very high level of stress. However, since subduction near Honshu does not follow a straight fault line along the tectonic boundary as defined by the Japan Trench, most large tsunamigenic earthquakes along the Sanriku region - even the most destructive - involve relatively short ruptures, but proportionately large slips. Although their seismic energy release may be quite high, the affected crustal blocks tend to be smaller because of existing asperities.

The 2011 earthquake – like most large earthquakes – had a complex rupture which exhibited a variation in velocity. The rupture propagation, duration, and displacements were investigated by numerous researchers using different models and techniques (Wang and Mori, 2011; Shao et al., 2011; Ammon et al., 2011). Accordingly, the earthquake ruptured the interplate boundary off-shore east Honshu, with fault displacements of up to 40 m, variable rates of propagation and a rupture duration which was estimated to range from 150 to 170 seconds. The estimates were relatively consistent. For example, data recorded by the dense USArray network in Japan, indicated that the quake exhibited a variable rupture propagation, which ranged from about 1.0 to 3.0 km/s for the high-frequency radiation and lasted approximately 170 seconds. Significant changes of physical properties along the fault plane may be the reason for the variability in the velocity of rupture propagation. The overall rupture length was estimated to be about 450 km long (Wang and Mori, 2011).

5.1.5 Examination of Seismic Energy Release

Inversion of teleseismic P waves and broadband Rayleigh wave observations with high-rate GPS recordings indicated a moment of $3.9 — 10^{22}$ Nm (Mw 9.0) and a centroid time of 71 s. (Ammon et al., 2011). Teleseismic body and surface wave analysis of both broadband body waves and long period seismic waves (Shao et al, 2011) determined the total seismic moment to be 5.8 — 1022 Nm. Furthermore, the resulting rupture models showed a steady increase of moment rate for the first 80 seconds and an initial rupture speed of 1.5 km/s mainly in a northwesterly direction. Subsequent rupturing in a southwestward direction continued at a speed estimated at about 2.5 to 3.0 km/s. As stated, changes in physical properties of crustal and sedimentary material may be responsible for the variation in speed. Usually, areas of low rupture velocity are associated with large energy release along the fault plane, while high rupture speed may be associated with lower energy release.

5.1.6 Examination of Crustal Movements

The 2011 earthquake was a megathrust event with the Pacific plate moving underneath the Eurasian plate. As a result, the landmass of Honshu Island moved in an east-southeasterly direction. Based on the Global Positioning System, the Geospatial Information Authority in Tsukuba, Japan, estimated that the Oshika Peninsula near the epicentral area moved by a little over 5 meters (17 feet) eastward and subsided by a little over 1 meter (4 feet). Additionally, the Geospatial Information Authority stated that there were land mass movements in many areas of Honshu, from the northeastern region of Tohoku to the Kanto region, including Tokyo. Slip and fault displacements were estimated to be up to 40 meters (Ammon et al., 2011). However, direct measurement of seafloor

deformation near the trench axis by JAMSTEC (Japan Agency for Marine Earth Science and Technology) indicated the average seafloor displacement of 50 m within the 40 km west of the trench axis. Such large slips near trench are not uncommon for great subduction earthquakes of Mw>8. Finally, based on the kinematic rupture history, it is estimated that a vertical uplift of up to 10 meters on the east side of the fault and nearer to the Japan Trench axis and asperity, was the cause of the destructive tsunami.

The existence of thrust earthquakes in this segment off Honshu indicates that either the sediments along the plate boundary become sufficiently well consolidated and dewatered at about 70 km from the deformation front, or that older, lithified rocks are present within the forearc so that stick-slip sliding behavior becomes possible when the stress exceeds a critical level. Fig. 9 , illustrates that the maximum slip occurred along a relatively shallow region ranging 140-180 km in length, in both directions above the quake's hypocenter. At the present time there is not sufficient data or surveys of the area to fully evaluate the effect of sediments on the subduction dynamics off the northeast coast of Honshu.
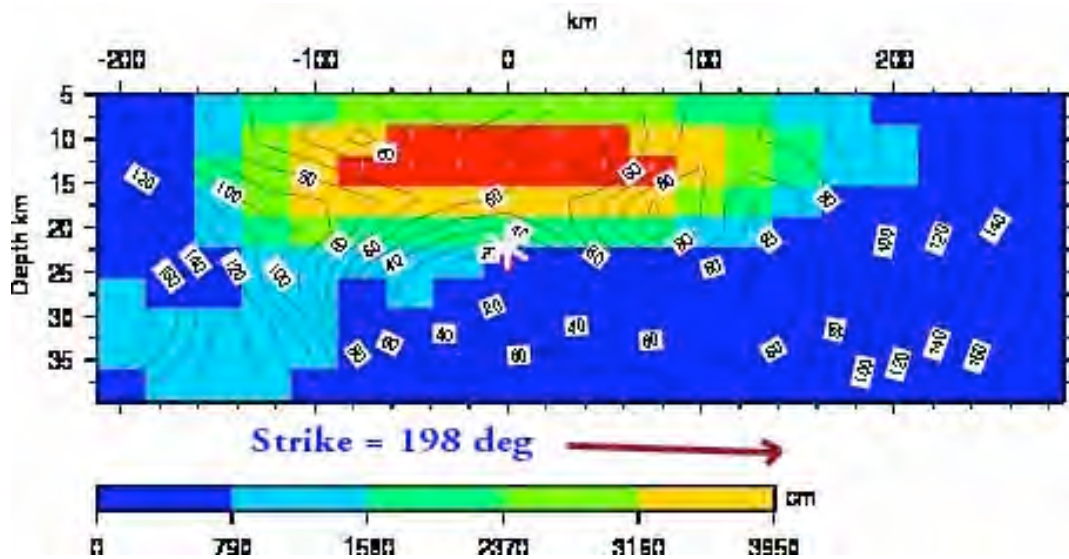

Fig. 9. Cross-section of the quake's slip distribution. The strike direction of the fault plane is indicated by the red arrow and the hypocenter location and depth of the March 11, 2011 earthquake are denoted by the white star. Contours show the rupture initiation time in sec. (modified after Shao et. al. 2011).

5.1.7 Tsunami Source Area

The 2011 Sanriku earthquake packed a great deal of energy. However, its tsunami generating source area was relatively small compared to those of the great Sumatra (2004) and Chile (2010) earthquakes (Pararas-Carayannis, 2005, 2010). The Sumatra earthquake had a rupture that propagated also at varying speeds along two segments of the Sunda tectonic boundary and its overall tsunami source area was almost 1,300 km long, about 300 km wide and involved large slip.
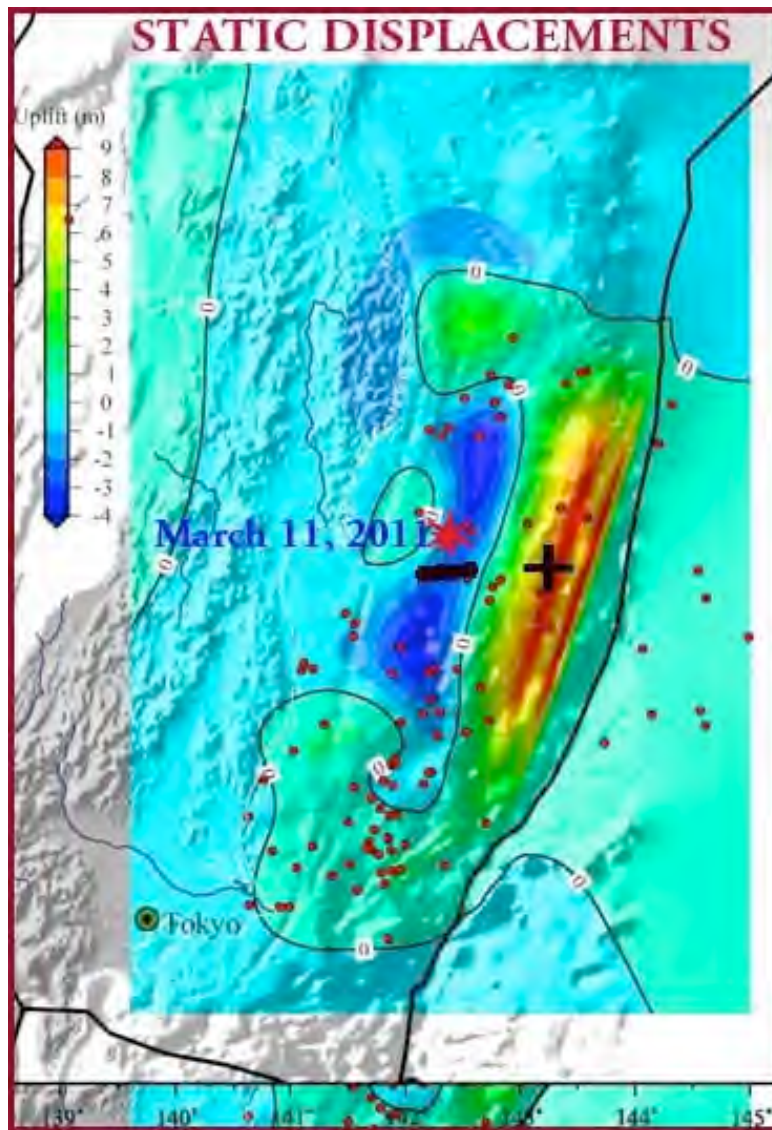
Fig. 10. Predicted Vertical Static Displacements (positive and negative) based on the inverted slip model (Cross-section of slip distribution shown in Fig indicating maximum tectonic uplift of almost 10 meters (modified after Shao et al. 2011).

By comparison, the 2011 Sanriku earthquake had an extensive aftershock region that was almost 450-km long and 200-km wide, but the source region that generated the large tsunami was rather compact. Focal mechanism analysis indicates dipole crustal movements involving both subsidence and uplift. Apparently, most of the positive vertical static displacements occurred closer to the Japan Trench on the accretionary prism (Fig. 10). Also, teleseismic P waves and broadband Rayleigh wave observations (Ammon et al., 2011) support the conclusion that most of the significant displacements that generated the larger tsunami occurred in the first 80 seconds after rupture initiation.

What contributed to the higher tsunami heights were the earthquake's up-dip rupture expansion, mainly above the quake's hypocenter (at 20-24 km depth), which resulted in extensive additional vertical and horizontal movements and uplift of sediments on the overriding plate - which extended almost to the edge of the Japan Trench. Although the overall tsunami source area was about 300 to 350-km long and about 150 to 175-km wide, the spatial and temporal sequencing and clustering of major aftershocks and the energy release indicate that the main source area that generated the higher tsunami was about 120-140 km long and about 80 km wide (Fig. 11).
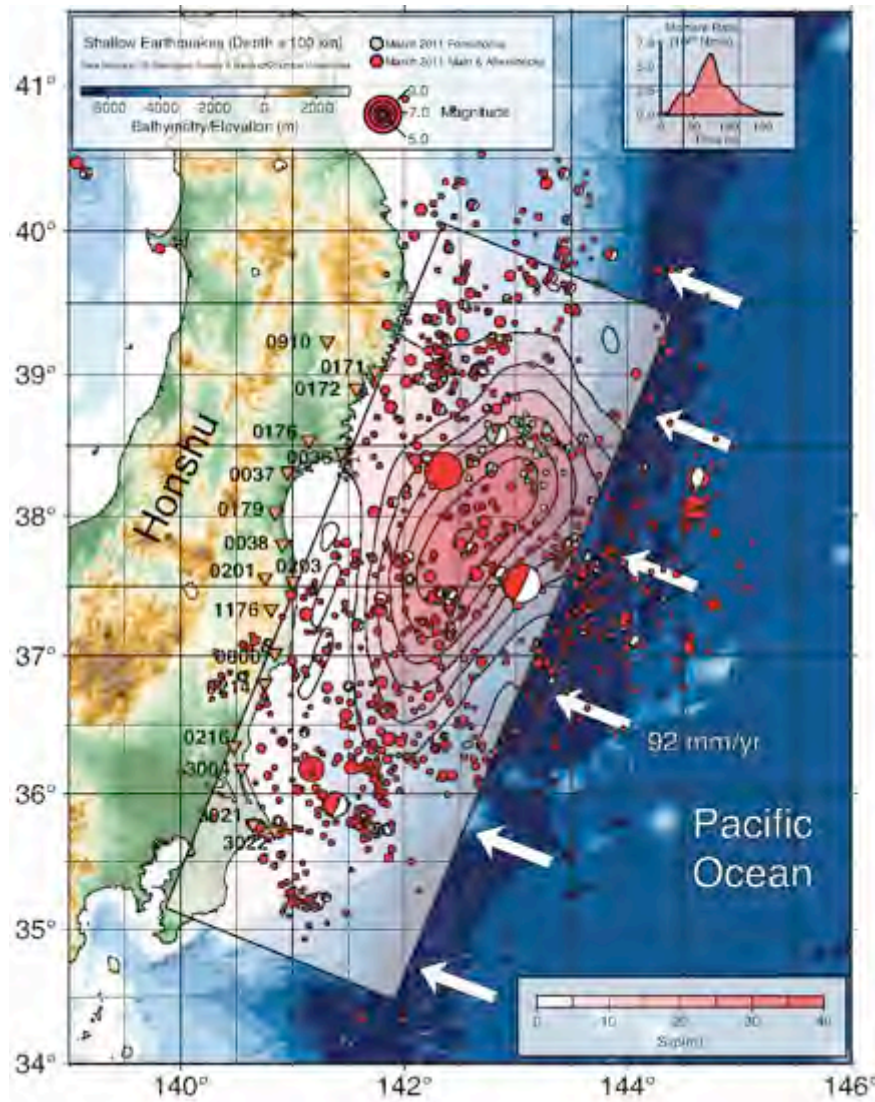
Fig. 11. Tsunami Generating Area showing the epicenter of the main earthquake on March 11, 2011, a major aftershock with magnitude 7.1 fifty minutes later and 172 aftershocks which were recorded by the USGS by March 12, 02:04:53 UTC 2011(After Ammon et al., 2011)

6.1.8 Tsunami Source Mechanism

Subduction of the Pacific tectonic plate beneath the Eurasian plate resulted in the great Sanriku earthquake of 2011. The earthquake involved primarily reverse thrust compression, as well as strike slip shear and east-southeast trending lateral movement of the overriding Japan volcanic arc of the Eurasian plate. The following source mechanism scenario is proposed to explain the larger height tsunami that struck northeastern coastal areas of Honshu and particularly the coasts of Miyagi and Fukushima Prefectures (Fig. 12).

Initial rupturing begun at the earthquake hypocenter focal depth of 24.4 km and expanded upward on the accretionary prism towards the ocean floor, first through well-compacted non-hydrated sedimentary layers and subsequently through fully hydrated layers. Rupturing continued in this manner for the first 80 seconds - propagating at the rate of about 1.5 km/sec for an approximate distance of about 120 km in a northwesterly direction from the epicenter location. The initial combination of reverse thrust compression, strike slip shear and east-southeast lateral movement and compression of the sedimentary prism, resulted in slip and fault displacements estimated to be up to 40 meters, maximum eastward movement of land mass estimated to be as much as 5 meters at the surface (17 ft. maximum near Oshika Peninsula) and subsidence estimated to be about 1.2 m.

Fig. 12. Postulated Crossection of the Accretionary Margin east of Honshu Island. Compression of the Sedimentary Prism and Subsequent Normal and Bookshelf Faulting contributed to the Tsunami's Source Mechanism and to greater Tsunamigenic Efficiency.

At first, the sediments on the accretionary prism along both east and west of the hypocenter compressed elastically. However the elastic deformation was short-lived, as in the next few seconds the rupturing process nucleated existing normal faults on the continental shelf on both sides of the rupture, which also begun to fail in sequence. Additionally, the reverse thrust motions and lateral compression ruptured the sedimentary layers of the accretionary prism, which begun failing sequentially in a bookshelf fashion creating several parallel and en-echelon thrust faults along a much

wider zone of deformation that extended westward toward the Japan Trench. Because of the lateral compression of the sedimentary layers and the subsequent failure due to bookshelf faulting, large volumes of sediments begun thrusting upward with fault dips becoming progressively steeper on the east side of the initial rupture and along the eastern zone of the accretionary prism closer to the Japan Trench. In this eastern region the greater volume of up-thrusted sediments contributed significantly to the generation of the higher tsunami that was generated in the first 80 seconds. Thus, the larger tsunami was generated along a zone of deformation that was about 120-140 km long and about 80 km wide off the coast of the Miyagi and Fukushima Prefectures – the regions that also experienced the greater tsunami devastation.

Subsequent rupturing in a southwestward direction continued for approximately 100 seconds at a speed estimated at about 3.0 km/s. for a total distance of about 300 kms. This region did not experience as much bookshelf faulting and there was lesser upward displacement of sediments and a smaller offshore tsunami. Thus the tsunami that struck coastal sites along the Ibaraki Prefecture was not as high. Studies of the rupture process in space and time (Honda et al., 2011) also confirm this conclusion.

7.   EVALUATION OF TSUNAMIGENIC EFFICIENCY

As stated, W-phase inversion indicated a moment of 3.9×10^{22} Nm (Mw 9.0) and a centroid time of 71 s. (Ammon et al, 2011). The back-projection method - which used data recorded on the USArray network (Wang and Mori, 2011) - estimated a rupture propagation with variable speed ranging from about 1.0 to 3.0 km/s for about 450 km in length in approximately 170 seconds.

The variable rupture propagation and change in directionality indicate that the tsunami generation area can be divided into two distinct segments along a wide zone of deformation. Apparently, the most significant disturbance of sediments occurred in the first segment when the rupture speed was slower and thus the tsunami height was greater. Since the two initial pulses occurred at 30 and 80 seconds in a rupture segment located 50 to 70 km northwest of the epicenter, we can conclude that the higher tsunami was generated along this segment during that time interval following the main earthquake. The third impulse which occurred about 250 km southwest of the epicenter about 180 seconds after the main shock, is indicative of higher rupture velocity in a southwestward direction from the quake's hypocenter and of second region of tsunami generation of much lesser height with lesser sediment contribution. The observed three-pulse energy release is also supported by the cluster algorithm analysis of the aftershocks, which indicates the segmentation of the tsunami generating area. As previously stated, there was a big cluster of 260 events, followed by a second cluster of 120 events and by third cluster of 60 events - as well as 20 very small clusters, most outside the tsunami generation area – some on the outer rise of the subducting tectonic plate (Fig. 7). These variations indeed reflect differences in the strength of physical properties on both the subducting and overriding tectonic plates – such as rigidity, compaction and degree of hydration/serpentinization - along the 450 km fault(s) that ruptured sequentially when the 2011 Tohoku earthquake struck.

Based on the above-described evaluation, we conclude that the great height of the 2011 tsunami along the Honshu's coastlines was caused by the crustal displacements due to up-thrust faulting and by the displacement and excessive uplift of sediments along the accretionary prism of the overriding tectonic plate, as it thrusted east-southeast towards the Japan Trench by as much as 5 meters (about 17 ft) in certain areas and probably more at the décollement depth. To what extent and what volume of sediments were uplifted cannot be estimated since the displacements were non-uniform over the entire length of the two main segments of the rupture zone. However, we can conclude that most of the sediment displacements occurred mainly along the segment of the fault off the Miyagi and Fukushima Prefectures where the seismic energy release was greater (Fig. 11). As stated, there was lesser seismic energy release along the segment off the Ibaraki Prefecture.

The amount of additional sediment uplift of the 1896 Sanriku earthquake (Fig. 13) was examined in the past (Tanioka & Satake, 1996; Tanioka & Seno, 2001). This event was characterized as a tsunami earthquake because of its slow rupturing velocity and weak ground motions along the Sanriku coast.

Fig. 13. Estimated earthquake fault parameters and generation area of the 1896 tsunami as determined by reverse wave refraction from three tide gauges in the region (modified original graphic by Tanioka & Satake, 1996; also shown in Tanioka & Seno, 2001 with a change of fault dip from 20 to 10 degrees). The sum of elastic deformation and the additional uplift of sediments were used with three different models of displacement to estimate total ocean floor deformation.

In trying to estimate the slip for this event by modeling, it was determined that a postulated 20° dipping fault along the top of the subducting plate, offered a match for both the observed seismic response and the tsunami, but required an estimated slip displacement of 10.4 meters. However, when a shallower fault dip of 10° was used and the additional uplift of sediments was taken into account, a slip ranging from 5.9 to 6.7 meters was obtained, which was in better agreement with the tsunami's waveforms recorded at three tide stations. By revising the fault modeling, Tanioka & Seno (2001) estimated the magnitude of the 1896 earthquake to be Mw=8.0-8.1. However, this was an underestimate as the magnitude of the 1896 earthquake was probably similar or even greater to that of 2011. Also, of the three displacement models they considered for the contribution of sediment uplift to tsunami generation, the one shown in Fig. 14   below - involving the only the leading edge of the accretionary prism - is more realistic but would still underestimate the actual sediment uplift of the 1896 tsunami. Apparently, the 2011 tsunami involved sediment uplift over a much wider area on the accretionary prism and thus it would be difficult to estimate quantitatively the effect on ocean surface displacement and wave heights at the source region.
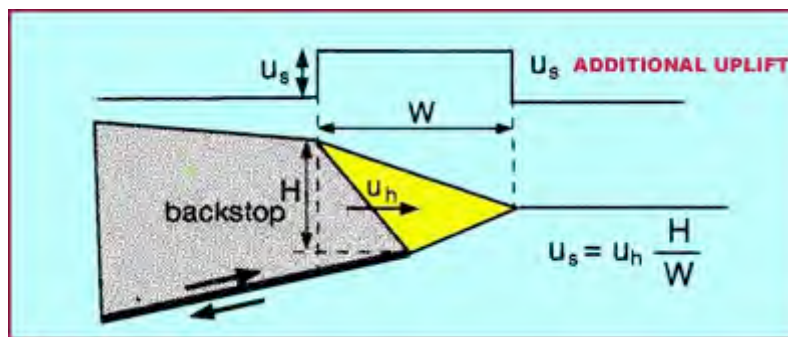

Fig. 14. Uplift of sediments by compressional forces. One of three models of displacements along the leading edge of the Accretionary Prism which was used to estimate additional contribution to tsunami height from a sediment uplift process for the 1896 event (modified after Tanioka & Seno, 2001).

8. EVALUATION AND COMPARISON OF THE 1896, 1933 AND 2011 SANRIKU EARTHQUAKES

The March 11, 2011 earthquake was one of the largest in the last century. Most recent great earthquakes struck Indonesia in 2004 and Chile in 2010. All of recent great earthquakes had rupture zones that extended for several hundred of kilometers and slips, which were 10 meters of more.

8.1.1 Destruction and Fatalities

Both the 1896 and the 2011 quakes generated extremely destructive tsunamis along the Sanriku coast. The 1933 tsunami was also very destructive (Iida et al., 1967; Hatori et al. 1982; Pararas-Carayannis, 2005). The estimated source region of the 1896 tsunami (Fig.) was somewhat north of that of 1833 and of 2011.

There were many similarities in the height of the tsunami waves and thus to the degree of destructiveness and the number of fatalities for all three events. For example, thirty to sixty minutes following the 1896 earthquake, tsunami waves begun to strike the Sanriku coastal region as well as the southern coasts of Hokkaido. The death toll of the tsunami was 26,360. At the village of Tarō only 36 people of its total population of 2,000 survived while all infrastructure and most of the houses were destroyed (Nakao, 2009). The 1933 tsunami was equally devastating. A total of 3,064 people were killed and 1,092 were injured. At Yoshihama, close to Ryori Bay, the 1933 tsunami was responsible for 982 deaths. The death toll of the 2011 tsunami was given as 13,843 at the end of April, with another 14,030 people missing. The impact of the Fukushima nuclear disaster may have a long-term collateral impact and will add to the total death toll.

8.1.2 Seismic Intensities

The great earthquakes of 1611 (Keichō), of 1896 (Meiji Sanriku) and of the 2011 (Sanriku) were not associated with strong ground motions over large areas but generated extremely devastating tsunamis. All three involved reverse faulting with slow rupturing within thick sedimentary layers. By contrast the 1933 "Showa" quake occurred on a normal fault.

The ground motions of the 1896 earthquake were not substantial and seismic intensities ranging from 2 to 4 were assigned to this event (JMA scale) for a relatively small area of Sanriku (Fig. 15). The quake's rupture velocity was relatively slow, indicating the presence of compacted sedimentary layers in the source region. However, the generated tsunami was extremely high, as this was a distinct tsunami earthquake with a slower fault slip than that which usually occurs during normal earthquakes. The ground motions of the 1933 earthquake were much stronger and were assigned an intensity of 5. However, the tsunami it generated was not as high as that of 1896. Although the 2011 event was also characterized as a tsunami earthquake, strong ground motions were felt as far away as Tokyo. The stronger ground motions were probably generated along the second segment of the earthquake's rupture, which was associated with higher propagation velocity of up to 3km/sec.
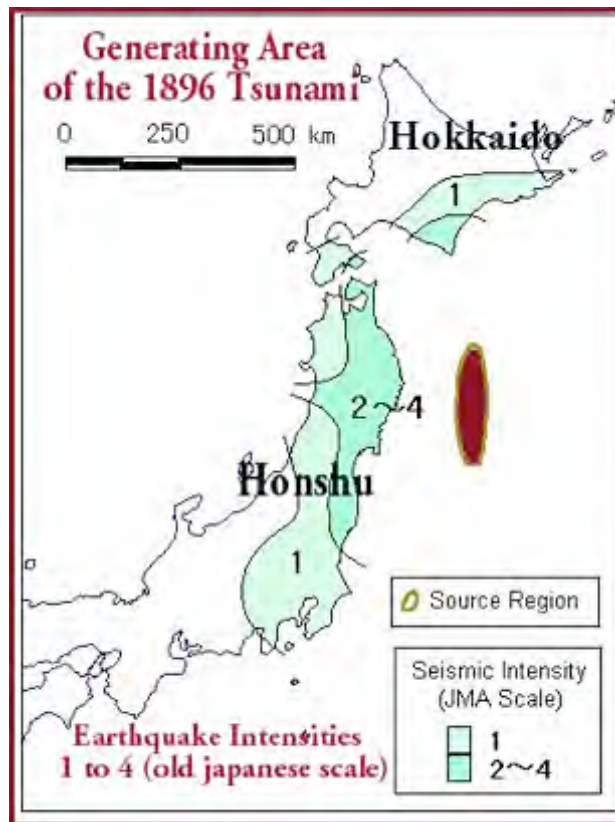
Fig. 15. Seismic Intensities of the 1896 Earthquake. Approximate generating area of the tsunami (modified after Japan Meteorological Observatory, 1896)

8.1.3 Source Mechanisms

Both the 2011 Sanriku earthquake and the 1896 "Meiji" earthquake occurred on reverse faults and had characteristics of severity of tsunami generation usually associated with slower initial fault slips and slow rupture velocities within compacted sedimentary layers. Both had slow rupture velocities initially - mainly within compacted sedimentary layers - thus resulting in greater vertical and horizontal displacements of sediments along the accretionary prism near the Japan Trench. Both events can be characterized as "tsunami earthquakes". By contrast the 1933 "Showa" quake occurred on a normal fault. Although this was also a great earthquake and generated a very destructive tsunami, its impact was not as severe as the 1896 and the 2011 events.

8.1.4 Tsunami Runup Heights

As stated, the March 11, 2011 tsunami impact on Honshu's coasts was similar to those of 1896 and 1933. All three tsunamis reached the shores of Honshu within 30 to 40 minutes after the main shocks were felt. The maximum heights for all three tsunamis occurred at Ryōri Bay in Sanriku, Iwate

Prefecture. The height of the 1896 tsunami was 38.2 meters, the highest ever in Japan since the tsunami of 1868 (Fig. 16). The maximum height of the 2011 tsunami was roughly the same as that of 1896, approximately 38 meters at the village of Ryōri. The 1933 tsunami in the same area reached a height of 23.0 m.
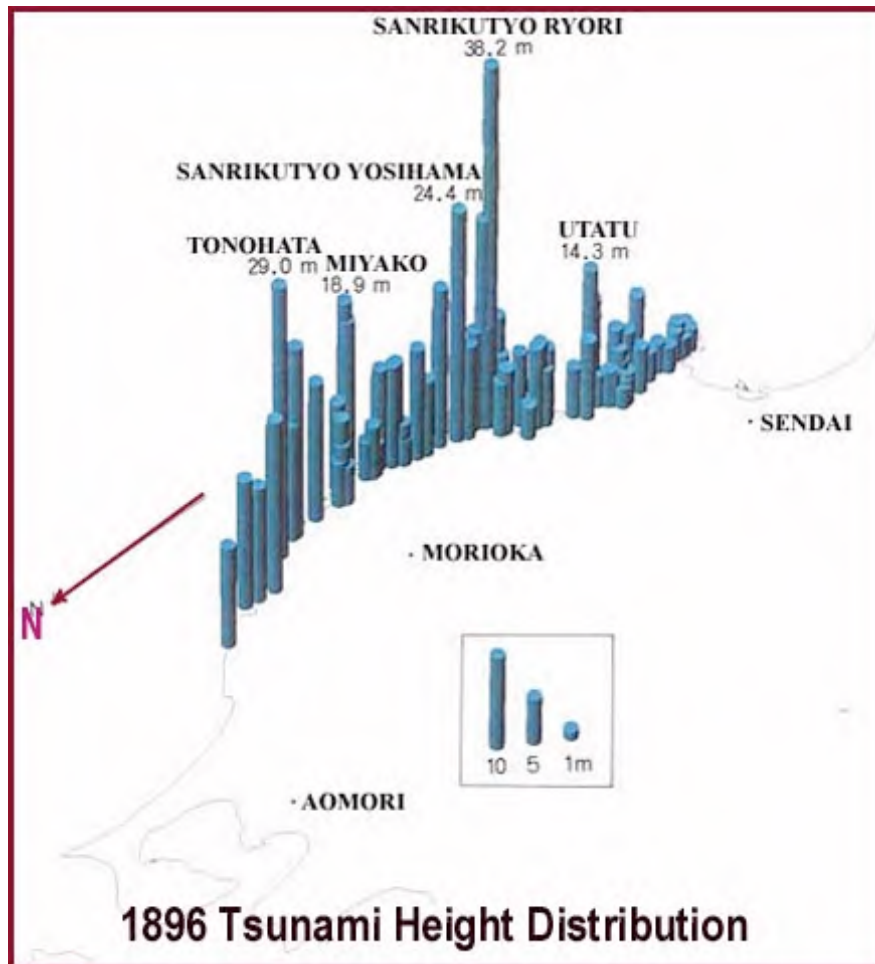

Fig. 16.   The *1896 Maximum Tsunami Height Distribution North of Sendai (modified after Hatori et al., 1982?)*

The far field impact of the 1896 tsunami was greater than that of 2011. In 1896, waves up to 9 meters (30 feet) struck the Hawaiian Islands, causing extensive destruction to wharves, boats and houses (Pararas-Carayannis, 1969). The waves of the 2011 tsunami were destructive but ranged from 2 to 3 meters (7 to 11 feet). Similarly in California a wave of about 3 meters (9.5 feet) was observed in San Francisco in 1896, but the 2011 was less and in Crescent City the maximum runup height of the 2011 tsunami was about 2.5 meters.

9. SUMMARY AND CONCLUSIONS

The anomalously high 2011 tsunami which occurred along Honshu's east coast resulted from a combination of crustal deformations of the ocean floor due to the upthrust tectonic motions of the earthquake, augmented by additional uplift due to large coseismic lateral movement which compressed and deformed sediments along the accretionary prism on the overriding tectonic plane near the Japan Trench. The event was a "tsunami earthquake" in the sense that it was mostly associated with a slow rupturing process and lateral movement within shallow and highly compacted sedimentary layers.

The deformation occurred randomly along parallel and en-echelon faults, which failed in a sequential bookshelf manner. Most of the energy release and deformations that generated the huge tsunami occurred along the shallow eastern segment of the fault off the Miyagi Prefecture, while the segment off the Ibaraki Prefecture – where the rupture process was rapid – released minor seismic energy and resulted in lesser compaction and deformations of the sedimentary layers. Because of the complexity of the rupturing process, the extent of additional uplift due to buckling of the sediments in the tsunami generation area off the Miyagi segment of the fault is difficult to estimate. However, both the 1992 Nicaragua and 2004 Sumatra earthquakes demonstrated that bookshelf failure of sedimentary layers could generate anomalously high tsunamis. Apparently, the same mechanism was responsible for the high tsunami generated in the offshore area off Honshu when the March 11, 2011 earthquake struck.

The great 1896 Sanriku earthquake was also a tsunami earthquake with a similar mechanism of tsunami generation enhanced by sediment deformation and uplift. Finally, the March 2011 event may have released most of the stress that had accumulated – thus ending a seismic cycle for this particular region off the Sanriku coast. However, due to energy transference, a new seismic cycle of stress has begun for the adjacent regions, which will culminate in another large tsunamigenic earthquake in the near future – perhaps in the next two to four years. A large tsunamigenic earthquake with moment magnitude up to Mw 8 can be expected to occur either to the north closer to Hokkaido and the Kurile Islands, or to the south closer to the Izu-Ogasawara Trench area.

REFERENCES

Ammon C. J., Thorne L., Kanamori H., Cleveland M., 2011. "A rupture model of the great 2011 Tohoku earthquake". Accepted May 18, 2011; Online published.

Hatori T., Aida I, Koyama M and T. Hibiya, 1982. Field Survey of the Tsunamis In Inundating Ofunato City - The 1960 Chile and 1933 Sanriku Tsunamis. Bull. of the Earthquake Research Institute, Vol. 57, pp. 133-150.

Honda R., Yukutake Y., Ito H., Harada M., Aketagawa T., Yoshida A., Sakai S. , Nakagawa S., Hirata N., Obara K. and Kimura H., 2011. "A complex rupture image of the 2011 Tohoku earthquake revealed by the MeSO-net". TERRAPUB Report (Received April 10, 2011; Revised May 18, 2011; Accepted May 29, 2011 and published Online).

Iida, K., D.C. Cox, and Pararas--Carayannis, G., 1967. Preliminary Catalog of Tsunamis Occurring in the Pacific Ocean. Data Report No. 5. Honolulu: Hawaii Inst. Geophys. Aug. 1967.

Kawakatsu, H., and T. Seno, 1983. Triple seismic zone and the regional variation of seismicity along the northern Honshu arc. J. Geophys. Res. 88 4215-4230, 1983.

Nakao, M., 2009. "The Great Meiji Sanriku Tsunami June 15, 1896 at the Sanriku coast of the Tohoku region". Retrieved 2009-10-18.

Pararas-Carayannis, G. 1992. The Earthquake and Tsunami of 2 September 1992 in Nicaragua http://drgeorgepc.com/Tsunami1992Nicaragua.html

Pararas-Carayannis, G. 1982. The historic record shows that a total of 65 destructive tsunamis struck Japan between A.D. 684 and 1960

Parras-Carayannis G. 1983, The Earthquake and Tsunami of 26 May 1983 in the Sea of Japan

Pararas-Carayannis, G., 1994. The Earthquake and Tsunami of July 12, 1993 in the Sea of Japan/East Sea - The Hokkaido "Nansei-Oki" Earthquake and Tsunami http://www.drgeorgepc.com/Tsunami1993JAPANOkushiri.html

Pararas-Carayannis, G., 2000. Major Earthquakes in Japan in the 20th Century http://drgeorgepc.com/EarthquakesJapan.html

Pararas-Carayannis, G., 2005. Earthquake and Tsunami of December 26, 2004, in Indonesia http://drgeorgepc.com/Tsunami2004Indonesia.html

Pararas-Carayannis G., 2006. Potential of Tsunami Generation along the Makran Subduction Zone in the Northern Arabian Sea, Case Study: The Earthquake and Tsunami of November 28, 1945, Science of Tsunami Hazards, Vol. 24, No. 5 pp 358-384

Pararas-Carayannis, G. 2006b. The Earthquake and Tsunami of 28 November 1945 in Southern Pakistan
http://drgeorgepc.com/Tsunami1945Pakistan.html

Pararas-Carayannis G., 2009. Earthquake and Tsunami of 3 March 1933 in Sanriku, Japan.
http://drgeorgepc.com/Tsunami1933JapanSanriku.html

Pararas-Carayannis G., 2010. Earthquake and Tsunami of 27 February 2010 in Chile - Evaluation of Source Mechanism and of Near and Far-field Tsunami Effects. Science of Tsunami Hazards, Vol. 29, No. 2. 2010. Also a summary at http://www.drgeorgepc.com/Tsunami2010Chile.html

Pararas-Carayannis, G., 2011a. The Great Tsunami of March 11, 2011 in Japan - Analysis of Source Mechanism and Tsunamigenic Efficiency. OCEANS 11, MTS/IEEE Proceedings, 2011

Pararas-Carayannis, G., 2011b. Earthquake and Tsunami of 11 March 2011 in Sanriku, Japan
http://www.drgeorgepc.com/Tsunami2011JapanSanriku.html

Seno, T. and D. G. Gonzalez, 1987. Faulting caused by earthquakes beneath the outer slope of the Japan Trench. J. Phys. Earth 35 381-407, 1987.

Seno, T. 1999a. Is northern Honshu a microplate? Tectonophysics 115 177-196 1985

Seno, T. 1999b. Syntheses of the regional stress fields of the Japanese islands The Island Arc 8 66-79 1999.

Seno, T., and Y. Yamanaka, 1996. Double seismic zones, compressional deep trench - outer rise events and superplumes in Subduction Top to Bottom, edited by G. E. Bebout, D. W. Scholl, S. H. Kirby, and J. P. Platt Geophys. Monogr. 96 347-355 1996

Seno, T., and Y. Yamanaka, 1998. Arc stresses determined by slabs: Implications for mechanisms of back-arc spreading. Geopys. Res. Lett. 25 3227-3230, 1998

Seno, T., T. Sakurai, and S. Stein, 1981. Can the Okhotsk plate be discriminated from the North American plate? J. Geophys. Res. 101 11305-11315, 1996

Seno, T., and B. Pongsawat, 1981. A triple-planed structure of seismicity and earthquake mechanisms at the subduction zone off Miyagi Prefecture, northern Honshu, Japan Earth Planet. Sci. Lett. 55 25-36, 1981

Seno, T., and G. C. Kroeger. 1983. A reexamination of earthquakes previously thought to have occurred within the slab between the trench axis and double seismic zone, northern Honshu J. Phys. Earth 31 195-216, 1983.

Seno, T., and T. Takano, 1996. Seismotectonics at the trench-trench-trench triple junction off central Honshu Pure Appl. Geophys. 129 27-40, 1989.

Seno, T., and Y. Yamanaka, 1996. Double seismic zones, compressional deep trench - outer rise events and superplumes in Subduction Top to Bottom, edited by G. E. Bebout, D. W. Scholl, S. H. Kirby, and J. P. Platt Geophys. Monogr. 96 347-355, 1996.

Shao, G., Li X., Ji C. and T. Maeda, 2011. Focal mechanism and slip history of 2011 Mw 9.1 off the Pacific coast of Tohoku earthquake, constrained with teleseismic body and surface waves, Earth Planets Space, submitted, 2011.

Tanioka, Y., and K. Satake (1996). Fault parameters of the 1896 Sanriku tsunami earthquake estimated from tsunami numerical modeling, Geophys. Res. Letters, 23-13,1549-1552.

Tanioka, Y.; Seno T. (2001). "Sediment effect on tsunami generation of the 1896 Sanriku tsunami earthquake". Geophysical Research Letters 28 (17): 3389–3392.

Wang D. and Mori J. 2011. "Rupture Process of the 2011 off the Pacific Coast of Tohoku Earthquake (Mw 9.0) as Imaged with Back-Projection of Teleseismic P-waves". *Earth Planets Space*, ******, 1–5, 2011

Wei D. and Seno T. 1998. Determination of the Amurian Plate Motion. In Mantle Dynamics and Plate Interactions in East Asia, edited by Martin Flower, GeoDynamics Series., AGU, 1998